Control of Drug-Excipient Particle Attributes with Droplet Microfluidic-based Extractive Solidification Enables Improved Powder Rheology

Denise Z. L. Ng [1,2,3] • Arif Z. Nelson [2,3] • Gareth Ward [4] • David Lai [5,6] • Patrick S. Doyle [2,7] • Saif A. Khan [1,3]

ABSTRACT

Purpose Industrial implementation of continuous oral solid dosage form manufacturing has been impeded by the poor powder flow properties of many active pharmaceutical ingredients (APIs). Microfluidic droplet-based particle synthesis is an emerging particle engineering technique that enables the production of neat or composite microparticles with precise control over key attributes that affect powder flowability, such as particle size distribution, particle morphology, composition, and the API's polymorphic form. However, the powder properties of these microparticles have not been well-studied due to the limited mass throughputs of available platforms. In this work, we produce spherical API and API-composite microparticles at high mass throughputs, enabling characterization and comparison of the bulk powder flow properties of these materials and greater understanding of how particle-scale attributes correlate with powder rheology.

Methods A multi-channel emulsification device and an extractive droplet-based method are harnessed to synthesize spherical API and API-excipient particles of artemether. As-received API and API crystallized in the absence of droplet confinement are used as control cases. Particle attributes are characterized for each material and correlated with a comprehensive series of powder rheology tests.

Results The droplet-based processed artemether particles are observed to be more flowable, less cohesive, and less compressible than conventionally synthesized artemether powder. Co-processing the API with polycaprolactone to produce composite microparticles reduces the friction of the powder on stainless steel, a common equipment material.

Conclusions Droplet-based extractive solidification is an attractive particle engineering technique for improving powder processing and may aid in the implementation of continuous solid dosage form manufacturing.

KEY WORDS microfluidics · particle engineering · pharmaceutical crystallization · powder properties · powder rheology

✉ Patrick S. Doyle
pdoyle@mit.edu

✉ Saif A. Khan
saifkhan@nus.edu.sg

[1] Department of Chemical and Biomolecular Engineering, National University of Singapore,
4 Engineering Drive 4., Singapore 117576, Singapore

[2] Critical Analytics for Manufacturing Personalized-Medicine, Singapore-MIT Alliance for Research and Technology, Singapore 138602, Singapore

[3] Campus for Research Excellence and Technological Enterprise, Singapore 138602, Singapore

[4] GSK Medicines Research Centre, Gunnels Wood Road., Stevenage, Hertfordshire SG12NY, UK

[5] GlaxoSmithKline LLC, Product and Process Engineering, 709 Swedeland Road., King of Prussia, Pennsylvania 19406, USA

[6] GlaxoSmithKline LLC, Advanced Manufacturing Technologies, 830 Winter Street., Waltham, Massachusetts 02451, USA

[7] Department of Chemical Engineering, Massachusetts Institute of Technology, Cambridge, Massachusetts 02139, USA

INTRODUCTION

In recent years, the pharmaceutical industry has made considerable advances in active pharmaceutical ingredient (API) synthesis via the development of novel chemistry routes [1, 2] and the implementation of continuous flow chemistry processes [3, 4]. Transitioning to continuous manufacturing allows for real-time monitoring and tuning to yield consistently high-quality products through an increased understanding of process parameters [5]. However, implementation of continuous oral solid dosage form manufacturing has been impeded by the poor powder flow properties of many API compounds [6–8]. In this work, we harness the combination of a high-throughput emulsification device and an extractive droplet-based particle synthesis method for the production of microparticles of a model hydrophobic API, artemether. By controlling the formulation and process parameters, we achieve scalable production of highly flowable API particles suitable for continuous solid dosage form manufacturing and gain insights into the relationships between particle attributes and powder rheology.

The pharmaceutical industry traditionally operates manufacturing lines in a batch-wise manner, where the product of each unit operation must undergo quality testing before it can be released to the subsequent unit operation along the manufacturing line [5, 9]. This leads to increased holdup, decreased productivity, and the need to rework or dispose of batches which do not meet regulatory specifications [5, 9–11]. Thus there is an increased drive towards the adoption of continuous pharmaceutical manufacturing due to the benefits of increased process understanding, and real-time tuning and monitoring [5]. Furthermore, the implementation of continuous manufacturing results in a smaller operational footprint, as the seamless flow of raw materials and products reduces the need for large holding containers between unit operations [5, 9]. For continuous solid dosage form production processes to function adequately, the flow properties of the API compound are extremely important. Poor flow properties of API compounds may necessitate the use of additional intermediate steps such as wet granulation, which increases the degradation risk of moisture-sensitive API compounds [12, 13], or roller compaction which increases the risk of heat-induced polymorphic transformation [8].

The powder flow properties of API compounds are a function of the API's polymorphic outcome [14], particle geometry [15, 16], particle size distribution [16], and composition [14]. Microfluidic droplet-based particle synthesis is an emerging particle engineering technique that allows for the production of monodisperse particles with the desired morphology, chemistry, and porosity [17, 18]. Crystalline neat or composite microparticles with controlled proportions of API and excipients [19, 20] can be generated by this technique, allowing for

control over API polymorphic outcomes [21], and dissolution profiles [19, 22]. The ability to directly control particle sizes via microfluidic droplet-based processing also circumvents the need for additional particle size alteration steps and minimizes polymorphic transformation risks. There have been reports on the use of co-processing of API and excipient to circumvent the poor processibility of API powders [23–26]. However, studies on the powder properties of microfluidics-generated API and API-excipient composite particles are limited due to the difficulty in scale-up to produce a minimum volume of powder required for flow testing [27].

In recent work, Fortt and coworkers demonstrated that the use of a high-throughput emulsification device enables a 100-fold increase in throughput for the extractive crystallization of cabotegravir in droplet-based microfluidic devices via a 40-channel parallelization [28]. However, the focus of their work was on the optimization of processing parameters for the production of spherical particles with structural integrity suitable for downstream processing. In this work, we build upon their demonstration by adopting the combination of high throughput emulsification and extractive-based crystallization on a different model hydrophobic API, artemether, and evaluating the observed range of bulk powder flow properties within the context of the observed particle attributes due to droplet-based processing.

Using a 90-channel emulsification device, we produce particles that are spherical agglomerates of neat artemether crystals (referred to as "artemether SA" henceforth) at a rate of up to approximately 240 g/day, sufficient for a variety of powder rheology tests. Through the incorporation of an excipient, polycaprolactone, we demonstrate control over the polymorphic form of artemether, which is a critical quality attribute, and produce these composite particles (referred to as "artemether PCL" henceforth) at a rate of approximately 672 g/day. To facilitate structure-to-rheology understanding, we then characterize the particle attributes such as the morphology, particle size distributions, and polymorphic forms of particles synthesized via the droplet-based platform, as well as the as-received artemether powder (referred to as "artemether raw" henceforth) and particles crystallized in the absence of droplet confinement (referred to as "artemether recrystallized" henceforth). Finally, we conduct a comprehensive series of industrial standard powder rheology tests including aeration, compressibility, shear cell, and wall friction tests to compare the performance of all the obtained powders in the context of their observed particle attributes. This understanding of how particle attributes influence powder rheology allows for the identification of critical particle attributes to be controlled during manufacturing. These results illustrate that droplet-based extractive solidification is an attractive particle engineering technique for improving powder processing and may aid in the implementation of continuous solid dosage form manufacturing.

EXPERIMENTAL SECTION

Materials

Ethyl acetate (HiPerSolv Chromanom) was purchased from VWR chemicals and used as received. Ultrapure water (18.3 MΩ) was obtained from a Millipore Milli-Q purification system. Artemether (TCI A2190) was purchased from Tee Hai Chemicals and used as received. Polycaprolactone (#19561) was purchased from Polysciences and used as received. Polyvinyl alcohol (MW ~ 67000) was purchased from Sigma Aldrich and used as received. Fluorinated ethylene propylene (FEP) tubing (0.01 in. inner diameter) and polytetrafluoroethylene (PTFE) tubing (1 mm I.D.) for the transportation of fluids were purchased from IDEX Health & Science LLC.

Methods

(i) *Synthesis of artemether and artemether composite microparticles*

For the synthesis of artemether SA, artemether was first dissolved in ethyl acetate at a concentration of 500 mg/mL; this constituted the dispersed phase. The continuous phase was composed of 2 wt% polyvinyl alcohol in ultrapure water. The dispersed phase and continuous phase were infused at 333 µL/min and 1000 µL/min respectively into a multichannel droplet generation module with syringe pumps (New Era syringe pump model: NE-4000 purchased from Achema Pte Ltd). The design of the multichannel droplet generation chip has been reported by Nisisako and coworkers [29] and the fabrication of the multichannel droplet generation module has been reported by Fortt and coworkers [28]. The generated droplets were then collected into a 1L ultrapure water reservoir in a conical flask to allow for the completion of ethyl acetate extraction into the continuous phase. The solid artemether microparticles were then suspended in ultrapure water and underwent Büchner filtration thrice before they were dried under vacuum at room temperature for 8 h.

The same procedure was repeated for the synthesis of artemether-PCL composites with modifications for the dispersed phase and the infusion flow rates for the dispersed and continuous phase. Artemether and polycaprolactone were dissolved at concentrations of 500 mg/mL and 250 mg/mL, respectively in ethyl acetate; this constituted the dispersed phase. The dispersed phase and continuous phase were infused at 150 µL/min and 450 µL/min respectively.

(ii) *Recrystallization of artemether in the absence of droplet confinement*

To evaluate the impact of particle geometry, artemether was recrystallized from ethyl acetate in the absence of droplet confinement. This was done following the procedure outlined by Xu and coworkers [30]. Artemether was first dissolved in ethyl acetate at a concentration of 500 mg/mL in a clean and dry 50 mL round-bottom flask, immersed in a water bath at 45 °C, on a heated stir plate. Thereafter, ethyl acetate was removed using a rotavap (model R-100 purchased from BUCHI Singapore Pte. Ltd.) by reduction of the pressure in the system, resulting in the formation of artemether crystals. The formed crystals were then vacuum dried at room temperature for 8 h before further characterization.

(iii) *Particle attribute characterization:*

(a) *Scanning electron microscopy*—Field emission scanning electron microscopy (FE-SEM) was used for structural characterization of the microparticles. A field emission scanning electron microscope (JEOL JSM-6700F) at 5 kV accelerating voltage was used to acquire further structural information on the microparticles. All samples were prepared on conventional SEM stubs with carbon tape and were coated with 10 nm of platinum by sputter coating.

(b) *Polymorphic characterization*—The polymorphic forms present in artemether Raw, artemether Recrystallized, artemether SA, and artemether PCL were determined via Differential Scanning Calorimetry (DSC) analysis and Powder X-ray Diffraction (PXRD). Around 5 mg of sample was crimped in a sealed aluminum pan and heated at 3 °C/min in the range of 40 to 120 °C with an empty sealed pan as a reference in a TA instruments DSC25 apparatus. Dry nitrogen was used as purge gas and the N_2 flow rate was 50 mL/min. An X-ray diffractometer (Bruker, D8 Advance) was operated at 40 kV, 30 mA, and at a scanning rate of 0.78°/min over a range of 2θ from 5 − 40°, using a Cu radiation wavelength of 1.54 Å.

(c) *Particle size characterization*—The particle sizes of artemether Raw and artemether Recrystallized were obtained by using the MATLAB function, "regionprops", on optical microscopy images. The obtained area of each particle was converted to an area-equivalent diameter and plotted as a histogram. Particle size distributions for artemether SA and artemether PCL were obtained via digital image analysis (using ImageJ, NIH), in which 100 particles' area was measured and converted into its equivalent diameter for each formulation. The circularity was calculated for each particle as,

(iv) *Powder rheology characterization*

The various types of powders were subjected to shear cell, wall friction, compressibility, and aeration tests on an FT4 powder rheometer (Freeman Technology, UK). For shear cell tests, powders were loaded into a 10 mL cylindrical shear cell and conditioned. The powder bed was then pre-consolidated at a normal stress of 3 kPa using a vented piston. Incipient shear stresses for flow

were obtained at normal stresses of 1, 1.25, 1.5, 1.75, and 2 kPa with a bladed shear head. A yield locus was plotted based on the recorded shear stress and normal stress values using the inbuilt FT4 analysis software. The wall friction test was conducted similarly using a 1.2 μm roughness stainless steel disc rather than the bladed shear head. For compressibility tests, powders were loaded into a 10 mL cylindrical cell and conditioned. The height of the powder bed was recorded for various normal stresses, ranging from 1 to15 kPa. The change in powder bed height was converted to volume change (%) and plotted against the various normal stresses. For aeration tests, powders were loaded into a 35 mL cylindrical cell with an aerated base and conditioned thrice. The air velocity was controlled via a mass flow controller auxiliary unit. An angled blade traversed downwards into the powder bed as the air flowed at air velocities of 2 to 20 mm/s at intervals of 2 mm/s. As the angled blade traversed downwards, the forces on the blade were measured and recorded. The force was integrated with the distance through which the bed traversed, and the resultant energy was plotted against various air velocities.

RESULTS AND DISCUSSION

Establishing a High Throughput Droplet-Based Extractive Solidification Process for Artemether

We first conducted droplet-based extractive solidification containing artemether or artemether-polycaprolactone solutions to yield spherical microparticles with narrow size distributions. In our previous works, we have established both microfluidic evaporative and extractive droplet-based processing techniques to convert API- or API-excipient-laden droplets into spherical microparticles (20, 22). In this work, we have chosen extractive droplet-based processing since it is simpler than evaporative processing and can be applied to heat-labile APIs. Extractive processing is driven by the solubility of the dispersed-phase solvent in the continuous phase and requires no heating. For the selection of partially miscible solvents, an ethyl acetate-water emulsion system was chosen as previous reports have established its use in the creation of API/API-excipient microparticles (22) and polymer capsules (31). Artemether, a heat-labile anti-malarial (32) and one of the APIs listed on the world's health organization list of essential medicines (33), was selected as the model API. Polycaprolactone was selected as the model excipient since it has been reported to be able to control the polymorphic form of some APIs (34) and allowed for a suitably high mass throughput (see Section 1 in the Supporting Information for more details).

To generate sufficient amounts of powders for rheological testing, a platform consisting of two modules: droplet generation and solidification, was used as shown in Fig. 1a. An image of the experimental setup can be found in the supporting information (See Figure S1 in supporting information for details). For droplet generation, we adopted a palm-sized silicon chip microfluidic droplet generator developed by Nisisako and coworkers, which can process up to 180 mL/hr of dispersed phase (29). This device allows droplets to be generated at much higher frequencies and mass throughputs compared to single-channel microfluidic devices, as shown in Fig. 1b and as demonstrated by Fortt and coworkers (28). The generated droplets flow through the central orifice in the droplet generator into a reservoir of ultrapure water, allowing the ethyl acetate to be fully extracted from the droplets and resulting in solidification into spherical artemether SA and artemether PCL. These particles were then filtered and vacuum dried. To verify that vacuum drying at room temperature for 8 h was an adequate drying time, 1H-NMR was performed to quantify the residual ethyl acetate in the particles and the relevant data are included in the Supporting Information (Section 3); briefly, the amount of residual ethyl acetate is less than 0.1% w/w and below the ICH guideline of 0.5% (35). With this method, we produce artemether SA at a rate of up to approximately 240 g/day, and artemether PCL at a rate of 672 g/day.

Powder Particle Attributes

To evaluate the effects of droplet-based processing on the morphology of the chosen model API, we obtained morphology information from the field emission scanning electron microscopy (FESEM) images on each of the obtained artemether powders. Figure 2 shows the FESEM images of all four samples whereas Fig. 3 shows the particle size distributions of the samples. The optical images used for particle size analysis are included in the supplementary information (See Figure S3 in Section 4 of Supplementary Information).

The artemether raw particles are equant shaped, and the particle size distribution follows a lognormal distribution with a mean of 50 μm and a standard deviation of 40 μm. The artemether recrystallized particles have irregular shapes and the particle size distribution follows a lognormal distribution with a mean of 144 μm and a standard deviation of 135 μm. On the other hand, particles synthesized via our droplet-based platform, artemether SA and artemether PCL, are observed to be spherical and have Normal particle size distributions. Artemether SA has a mean of 132 μm and a standard deviation of 6 μm, whereas artemether PCL has a mean of 175 μm and a standard deviation of 12 μm. Polydispersity index, which is taken as the square of the ratio of the standard deviation to the mean, was also calculated for all the samples. The polydispersity indices of artemether raw, artemether recrystallized, artemether SA, and artemether PCL were 0.644, 0.868,

Fig. 1 (**a**) A schematic of the experimental setup used for generation of spherical artemether and artemether-polycaprolactone particles (**b**) Optical microscopy image of the circled portion in (a) of a 90-channel chip producing monodisperse artemether-laden droplets at a flow rate of 333 μL/min with 3 wt% PVA in ultrapure water as the continuous phase at a flow rate of 1 mL/min (**c**) A heap of free-flowing artemether-polycaprolactone composite powder.
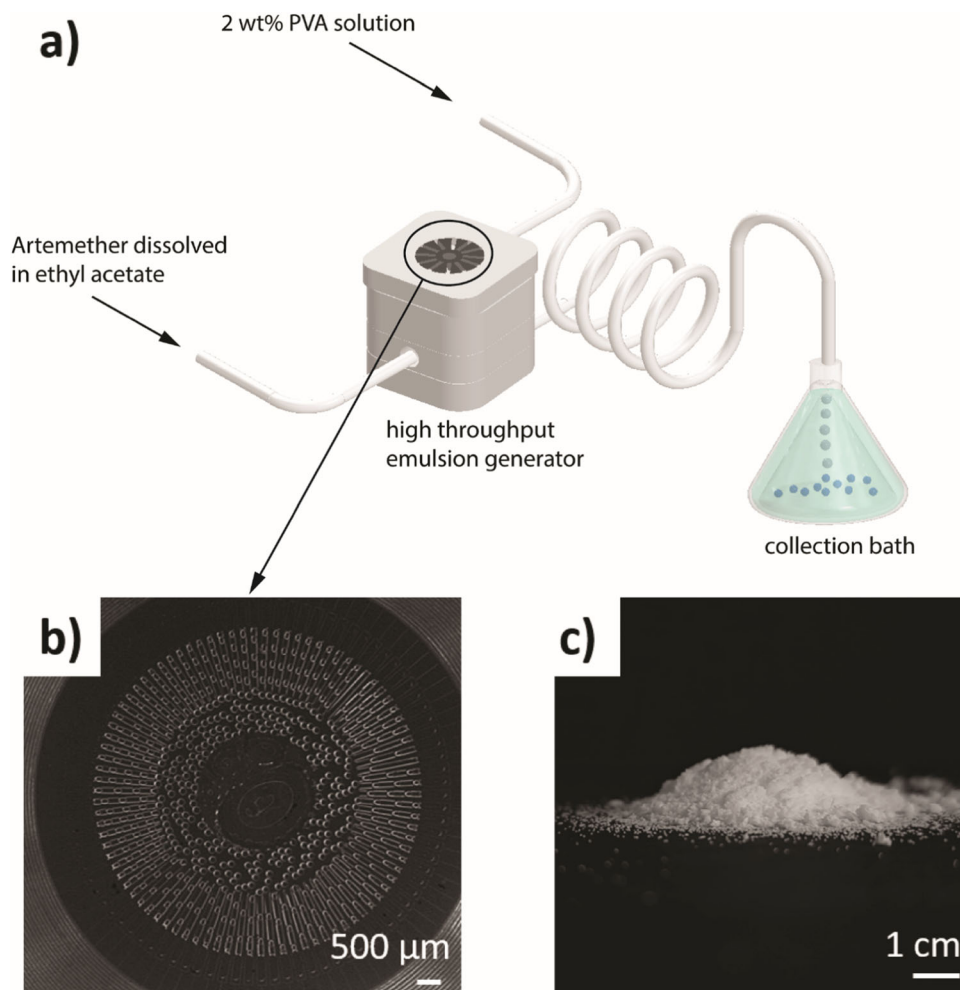
0.001, and 0.004. The average circularity of artemether raw, artemether recrystallized, artemether SA, and artemether PCL were 0.729, 0.634, 0.998, and 0.999 respectively. Both microfluidic droplet-based synthesized artemether SA and artemether PCL were observed to have reduced polydispersity and are highly spherical, due to the initial monodispersity of the generated droplets.

The polymorphic form of an API determines its ability to plastically deform under stress and the functional groups that are exposed at the particle surface (7). This in turn influences the powder's compression and flow behavior (7). Thus, the polymorphic forms of artemether present in the different types of particles were characterized using powder X-Ray Diffraction (PXRD) and differential scanning calorimetry (DSC) as shown in Fig. 4. Artemether raw and artemether PCL particles were ascertained to contain form A based on their PXRD spectra (36). The DSC thermogram of artemether raw shows a melting point at 86.8 °C, close to the reported melting point of form A, 86 °C (30). The DSC thermogram of artemether PCL shows a depressed melting point at 83.6 °C and an additional melting point at 54.1 °C

due to the presence and melting of polycaprolactone (37). Artemether recrystallized and artemether SA particles were ascertained to contain form B based on their PXRD spectra (36). The DSC thermograms of artemether recrystallized and artemether SA shows higher melting points at 87.9 and 89.4 °C respectively, close to the reported melting point of form B at 89 °C (30) The different polymorphic forms present in artemether raw and artemether recrystallized are likely due to the different solvents from which they were crystallized (30).

Effects of Particle Geometry, Polymorphic Form, Composition, and Particle Size Distribution on Powder Rheology

Shear Cell Behavior

Powder flow is a function of the intrinsic material properties of the powder, as well as the environmental conditions the powder is subjected to. We characterized the powder flow using several standard tests including stability, shear cell, wall friction, compressibility, and aeration. All powder samples' total
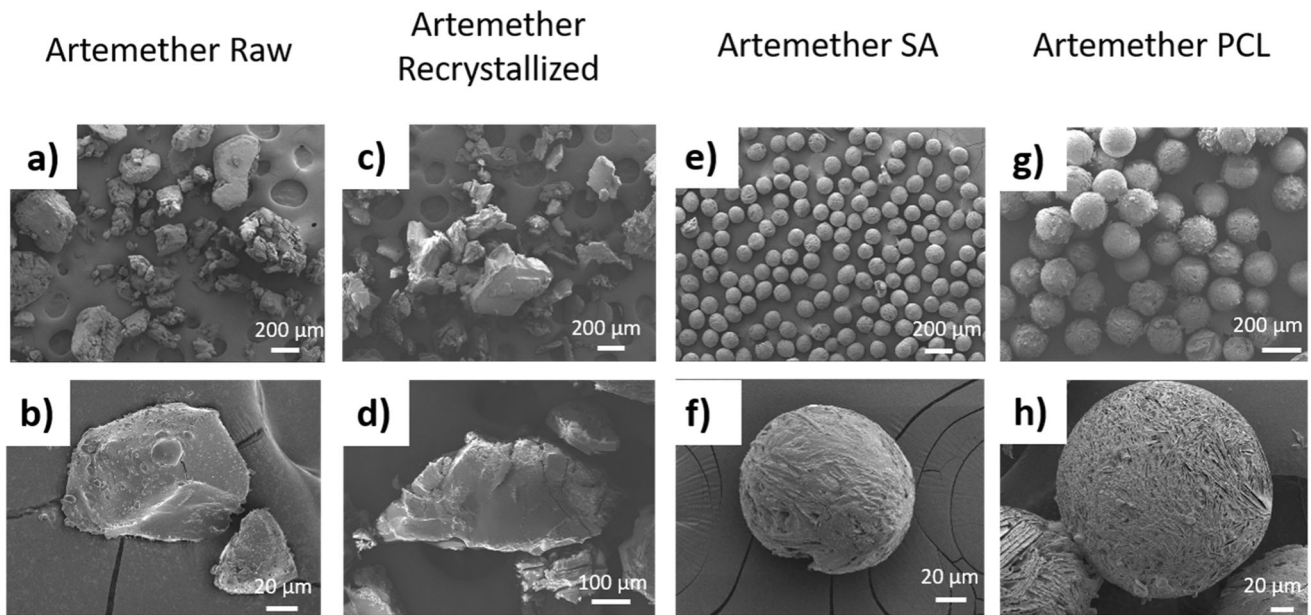
Fig. 2 Field emission scanning electron microscopy images of (**a-b**) as-received artemether (Artemether Raw) (**c-d**) artemether recrystallized via solvent evaporation (Artemether Recrystallized) (**e–f**) microparticles of spherical agglomerates of artemether from droplets containing artemether at 500 mg/mL (Artemether SA), (**g-h**) artemether-polycaprolactone microparticles from droplets containing artemether at 500 mg/mL and polycaprolactone at 250 mg/mL (Artemether-PCL). Particles produced from the droplet-based process, Artemether SA and Artemether-PCL, are highly spherical whereas the non-droplet-based particles, Artemether Raw and Artemether Recrystallized, are equant shaped.

flow energy remained constant during the stability test, indicating the stability of the particles to mechanical testing. (See Figure S4 in Section 5 of the Supporting Information for details).

The results of the shear cell characterization are shown in Fig. 5a and Table I. All four samples have very similar values

of angle of internal friction and density. The conditioned bulk density is measured after the powders have undergone a standard conditioning process on the FT4 rheometer. After conditioning, the powder bed is consolidated at a normal stress of 3 kPa to obtain the bulk density measurement. We used 3 kPa as the consolidation stress as most pharmaceutical unit

Fig. 3 Particle size distributions of (**a**) Artemether Raw (**b**) Artemether Recrystallized (**c**) Artemether SA and (d) Artemether PCL.
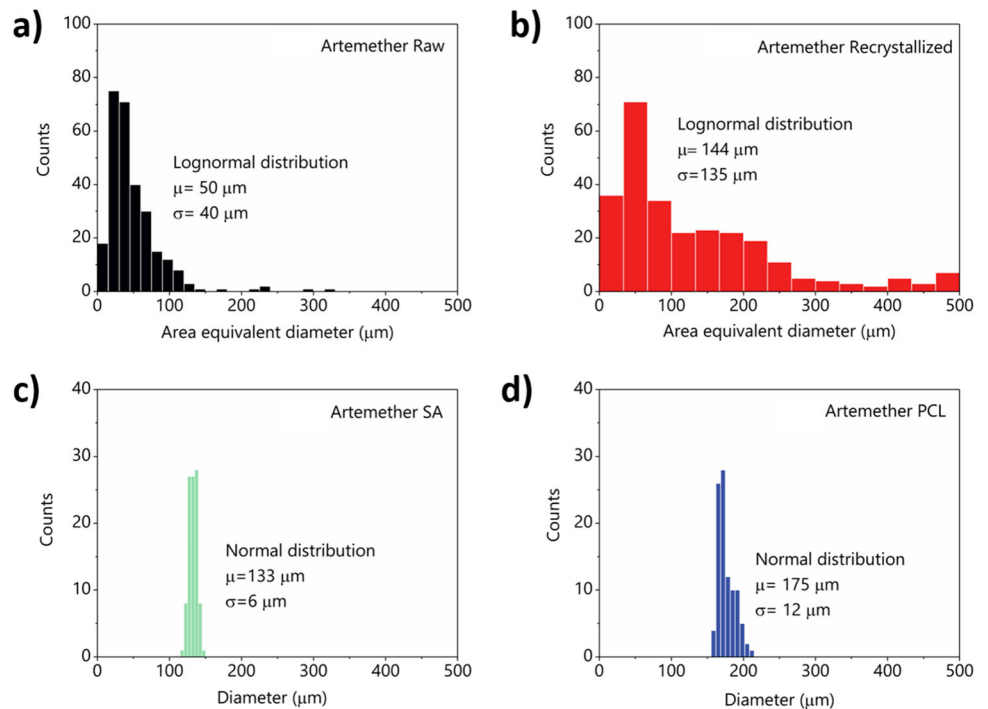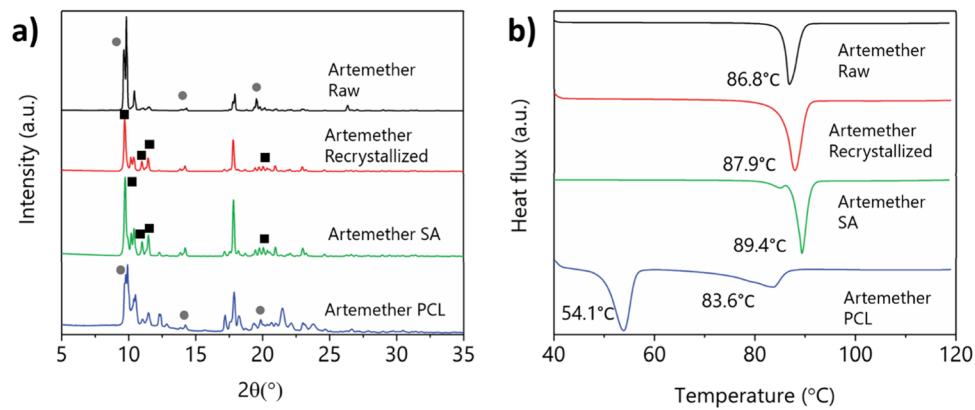
Fig. 4 (**a**) Powder X-ray diffraction (PXRD) spectra of artemether from Artemether Raw, Artemether Recrystallized, Artemether SA, and Artemether PCL. The spectra of the two reported forms of artemether have many similar peaks. The spectra of Artemether Raw and Artemether PCL match form A whereas the spectra of Artemether Recrystallized and Artemether SA match form B. ● denotes the characteristic peaks of form A whereas ■ denotes the characteristic peaks of form B. The PXRD spectrum of Artemether PCL exhibits two additional peaks at 21.3° and 23.5° which correspond to neat polycaprolactone particles. The PXRD spectrum of neat polycaprolactone particles is provided in Supplementary Information—Section 5. (**b**) Differential scanning calorimetry (DSC) thermograms of Artemether Raw, Artemether Recrystallized, Artemether SA and Artemether PCL. The melting point of artemether in Artemether Raw at 86.8 °C corresponds to the form A melting point (30). The melting point of artemether in Artemether Recrystallized and Artemether SA at 87.9 °C and 89.4 °C, correspond to the form B melting point (30). The lowered melting point for artemether within Artemether PCL at 83.6 °C is likely due to the presence of polycaprolactone, which melts at 54.1 °C.

operations have consolidation stresses below 6 kPa (38). Greater and smaller Mohr's circles were fit to the data in Fig. 5a to obtain the maximum principal stress and unconfined yield stress, the ratio of which is defined as the flow factor (See Figure S4 in Supporting Information for details), a numerical representation of flowability. The results show that the non-droplet-based particles, artemether raw, and artemether recrystallized, are more cohesive and are less flowable than the droplet-based artemether SA and artemether PCL. Artemether recrystallized is the most cohesive (cohesion value of 0.58 kPa), and the least flowable (flow factor, 3.57) of the four samples. Artemether PCL and artemether SA have low cohesion values of 0.14 kPa and 0.17 kPa, and the highest flow factors of 11.24 and 11.57 respectively, classifying the powders as "free-flowing" (39).

The markedly improved flow factor of artemether SA compared to artemether raw could be attributed to the differences in the particle morphology, polymorphic form, and particle-size distribution. Although artemether recrystallized and artemether SA were processed using the same solvent and resulted in the same polymorphic form, artemether recrystallized is more cohesive and has a lower flow factor than artemether SA. This is most likely due to the particle morphology. The equant shaped recrystallized artemether particles have numerous flat surfaces whereas artemether SA particles are highly spherical, resulting in a smaller contact area between artemether SA particles. Furthermore, the higher polydispersity index of artemether recrystallized and artemether raw results in more particle interlocking behavior and could account for the higher cohesion and lower

Fig. 5 (**a**) Incipient shear stress of powder flow as a function of the applied normal stress at a pre-consolidation stress of 3 kPa. The inset schematic depicts the test set-up with a 10 mL shear cell. (**b**) Incipient shear stress of powder flow as a function of the applied normal stress at a pre-consolidation stress of 3 kPa for wall friction tests. The shear cell was replaced with a stainless steel disc with a roughness of 1.2 μm. The wall friction angle was calculated as the inverse tangent of the gradient.
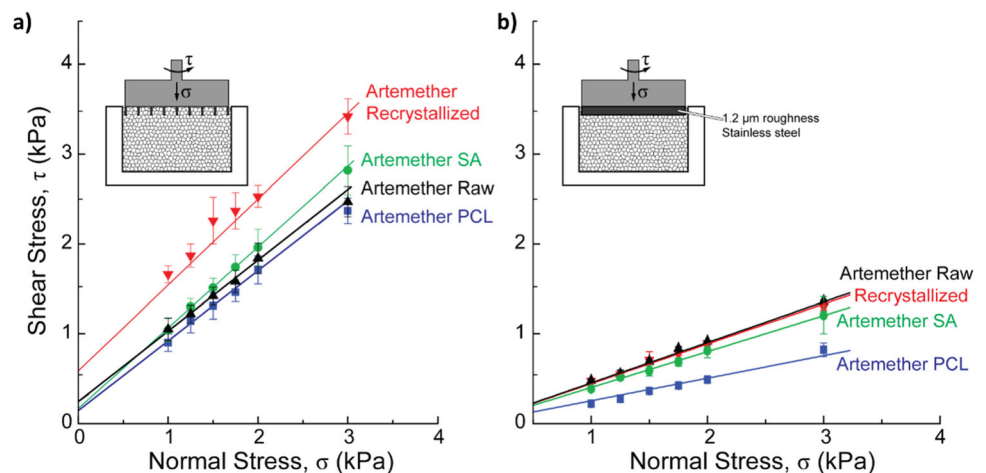
Table I Bulk Powder Properties of the Various Types of Powders as Measured in the Shear Cell and Wall Friction Test

Material	Cohesion (kPa)	Unconfined Yield Stress (kPa)	Major Principal Stress (kPa)	Flow Factor	Flow Behavior	Angle of Internal Friction (°)	Bulk Density (g/mL)	Conditioned Bulk Density (g/mL)	Wall Friction Angle (°)
Artemether Raw	0.24	1.00	6.63	6.62	Easy-flowing	38.21	0.63	0.525	24.44
Artemether Recrystallized	0.576	2.69	9.61	3.57	Cohesive	43.70	0.52	0.490	24.01
Artemether SA	0.17	0.74	8.32	11.24	Free-flowing	41.88	0.61	0.586	21.81
Artemether PCL	0.14	0.57	6.61	11.57	Free-flowing	37.84	0.57	0.508	14.20

flowability observed when compared against artemether SA and artemether PCL. Therefore, droplet-based extractive solidification of artemether can be used as a processing method to control particle attributes and improve flowability.

We also observed that artemether recrystallized is less flowable and more cohesive than artemether raw. This may be due to the lower circularity and higher polydispersity of artemether recrystallized, resulting in greater particle interlocking as compared to artemether raw. The difference in polymorphic forms may also result in different functional groups being exposed at the particle surfaces and play a role in the lower flowability observed as well (36).

Wall Friction Test

In oral solid dosage form manufacturing, powders frequently flow through hoppers in two different modes, mass flow or funnel flow (40). Mass flow is an ideal flow regime as the powder moves consistently in a first-in, first-out manner. In the funnel flow mode, regions of the powder that are in direct contact with the hopper remain stagnant and only powder in the center flows through the hopper. Several key parameters that control the powder flow regime are the powder angle of internal friction, hopper angle, and wall friction angle (40). Generally, the lower the wall friction angle, hopper angle, and powder angle of internal friction, the more likely the system will fall into the mass flow regime (40). The wall friction angle can be measured by replacing the shear cell with a disc that is made up of the intended wall material and carrying out a similar procedure to that of the shear cell test.

In this wall friction test, a stainless steel disc with a roughness of 1.2 μm was used as the model wall material. Figure 5b shows the plot of the shear stress required for the powder to flow at various normal stresses. The wall friction is calculated from the gradient of the best-fit line and is listed in Table I. The wall friction angle of artemether raw and artemether recrystallized are similar due to the materials' similarity in both particle shape and composition. There is a decrease in wall friction angle from 24° for the non-droplet-based particles to 22° for artemether SA and 14° for artemether PCL. The reduction in friction angle for artemether SA is likely due to a reduction in surface area in contact with the stainless steel disc as the particles are highly spherical. The further reduction in friction angle to 14° for artemether PCL is likely due to the differences in material composition at the particle surface. Visually, the surfaces of the artemether PCL particles do not appear substantially smoother than the artemether SA particles (Fig. 2f,h), therefore the reduction in friction between these two spherical particles is likely due to the reduced interaction strength of the PCL polymer with the wall material. Thus, co-processing of an API with an excipient during particle synthesis is an effective method for ensuring a mass flow regime occurs within powder hoppers.

Compressibility Test

Powders are also subjected to compressive stresses under various conditions such as storage in intermediate bulk containers and during compaction. Compressibility is a property that correlates inversely with the packing efficiency of the powder (39). It is generally preferable for powders to pack efficiently since this allows for the design of smaller holding containers and it enables the manufacturing of high dosage API tablets that are smaller and easier to swallow (41, 42). Figure 6a depicts the powder compressibility as a function of applied normal stress. The droplet-based powders, artemether SA and artemether PCL, have lower compressibility than the non-droplet-based powders, indicating that their volume does not decrease substantially with applied normal stress. We attribute this to the improved monodispersity and spherical shape of the droplet-based particles. The improved morphology allows these particles to pack in a random close-packed fashion and are thus already close to their maximum bulk density.

Aeration Test

Air entrainment is also an aspect of powder behavior that influences solid oral dosage form manufacturing. For example, fluidization is a common unit operation used to dry powders and coat granules (43). Furthermore, powders may be pneumatically conveyed between different unit operations to maintain sterility and reduce the risks of industrial hygiene-associated illnesses. Figure 6b shows a plot of total flow energy during aeration–the energy required to move an angled blade through the aerated powder bed—as a function of imposed air velocity. Except for artemether recrystallized, all of the powders' aeration energy reduces with increasing air velocities and eventually plateau. This suggests that artemether raw, artemether SA, and artemether PCL can be fluidized at higher air velocities whereas artemether recrystallized is unable to be fluidized. This also suggests that artemether recrystallized is the most cohesive of all samples, which is consistent with our shear cell experiments "Shear cell behavior".

CONCLUSIONS

In this work, we presented a detailed study on the attributes and powder rheology of monodisperse spherical crystalline artemether particles and artemether PCL composite particles and a comparison of these powders to the conventional non-droplet-based particles. The production of sufficient amounts of monodisperse spherical crystalline particles for rheological characterization was enabled by adopting a 90-channel droplet generation chip and the usage of an extractive droplet-based processing technique. This experimental setup can be scaled up even further by increasing the number of channels.
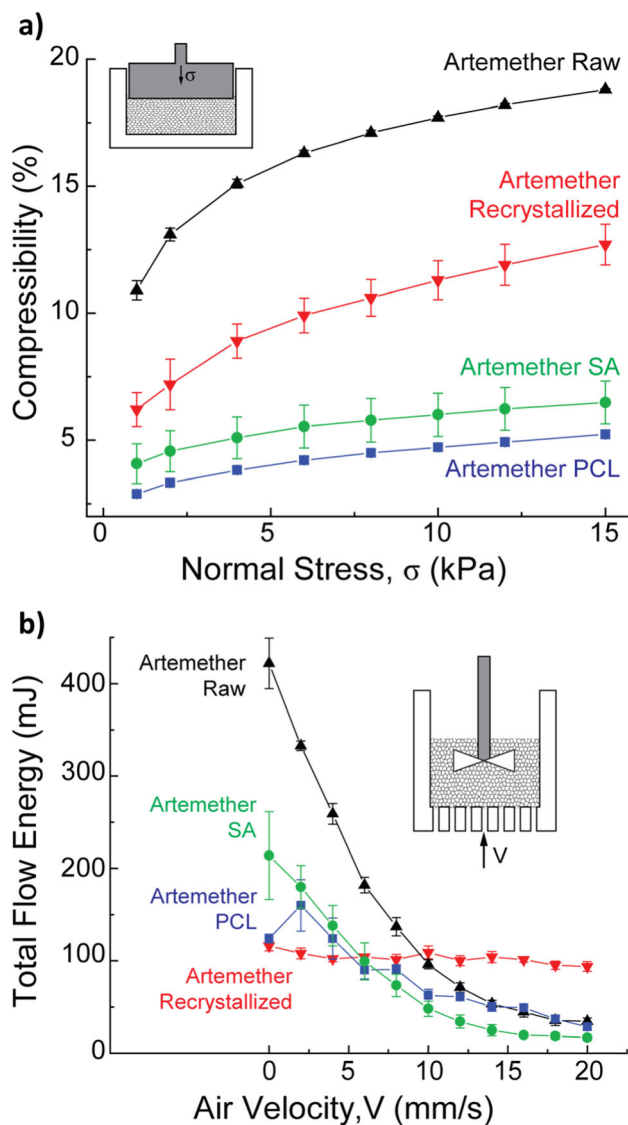

Fig. 6 (**a**) Compressibility percentage versus applied normal stress. Compressibility is calculated as the percentage volume change of the powder bed. The inset schematic depicts the test setup. (**b**) Aeration test results showing the total flow energy of the various powders versus air velocity. The inset schematic depicts the test setup.

One potential device is the silicon and glass very large scale droplet integration device, which houses 10,260 droplet generators, developed by Yadavali and coworkers (44). Assuming that the dispersed phase flow rate through each channel is kept constant, using Yadavali's device would allow us to achieve a throughput of ~ 27 kg/day, allowing us to approach the tonne/year throughputs which are typical of small molecule APIs. Although the experimental setup presented was semi-batch, a fully continuous form of this system can also be envisioned by having solutions infused from a reservoir with the use of HPLC pumps or alternating pressure vessels, the use of continuous filtration to isolate particles, and infusion of fresh ultrapure water into the solidification unit to ensure sink conditions are continuously maintained. The filtered particles

could then be dried in fluidized bed dryers or vacuum tumble bed dryers as these dryers provide slight agitation to prevent bridge formation between particles and drying to occur under minimal heat. We characterized the bulk powder properties of the droplet synthesized particles and the non-droplet synthesized particles, and discussed them with consideration of particle attributes. The superior bulk powder properties exhibited by the droplet-based spherical particles, and the mass throughputs enabled by this method highlight the potential in employing droplet-based crystallization to control particle attributes and improve processing ease for downstream pharmaceutical manufacturing.

AUTHORS' CONTRIBUTIONS

All authors contributed to the study conception and design. Material preparation, and data collection were performed by D.Z.L.N. Data analysis was performed by D.Z.L.N and A.Z.N. The first draft of the manuscript was written by D.Z.L.N and A.Z.N. All authors commented on previous versions of the manuscript, read, and approved the final manuscript.

Publisher's Note Springer Nature remains neutral with regard to jurisdictional claims in published maps and institutional affiliations.

REFERENCES

1. Li H, Tang X, Pang JH, Wu X, Yeow EKL, Wu J, et al. Polysulfide anions as visible light photoredox catalysts for aryl cross-couplings. J Am Chem Soc. 2021;143(1):481–7. https://doi.org/10.1021/jacs.0c11968.

2. Sambiagio C, Noël T. Flow photochemistry: shine some light on those tubes! Trends Chem. 2020;2(2):92–106. https://doi.org/10.1016/j.trechm.2019.09.003.

3. Porta R, Benaglia M, Puglisi A. Flow chemistry: recent developments in the synthesis of pharmaceutical products. Org Process Res Dev. 2016;20(1):2–25. https://doi.org/10.1021/acs.oprd.5b00325.

4. Adamo A, Beingessner RL, Behnam M, Chen J, Jamison TF, Jensen KF, et al. On-demand continuous-flow production of pharmaceuticals in a compact, reconfigurable system. Science. 2016;352(6281):61. https://doi.org/10.1126/science.aaf1337.

5. Domokos A, Nagy B, Szilágyi B, Marosi G, Nagy ZK. Integrated continuous pharmaceutical technologies—a review. Org Process Res Dev. 2021. https://doi.org/10.1021/acs.oprd.0c00504.

6. Schenck L, Koynov A, Cote A. Particle engineering at the drug substance, drug product interface: a comprehensive platform approach to enabling continuous drug substance to drug product processing with differentiated material properties. Drug Dev Ind Pharm. 2019;45(4):521–31. https://doi.org/10.1080/03639045.2018.1562467.

7. Chattoraj S, Sun CC. Crystal and particle engineering strategies for improving powder compression and flow properties to enable continuous tablet manufacturing by direct compression. J Pharm Sci. 2018;107(4):968–74. https://doi.org/10.1016/j.xphs.2017.11.023.

8. Govindarajan R, Suryanarayanan R. Processing-induced phase transformations and their implications on pharmaceutical product quality. Polymorphism. 2006:333–64. https://doi.org/10.1002/3527607889.ch13.

9. Schaber SD, Gerogiorgis DI, Ramachandran R, Evans JMB, Barton PI, Trout BL. Economic analysis of integrated continuous and batch pharmaceutical manufacturing: a case study. Ind Eng Chem Res. 2011;50(17):10083–92. https://doi.org/10.1021/ie2006752.

10. Domokos A, Nagy B, Gyurkes M, Farkas A, Tacsi K, Pataki H, et al. End-to-end continuous manufacturing of conventional compressed tablets: From flow synthesis to tableting through integrated crystallization and filtration. Int J Pharm. 2020;581:119297. https://doi.org/10.1016/j.ijpharm.2020.119297.

11. Vargas JM, Nielsen S, Cardenas V, Gonzalez A, Aymat EY, Almodovar E, et al. Process analytical technology in continuous manufacturing of a commercial pharmaceutical product. Int J Pharm. 2018;538(1–2):167–78. https://doi.org/10.1016/j.ijpharm.2018.01.003.

12. Waterman KC, Adami RC, Alsante KM, Antipas AS, Arenson DR, Carrier R, et al. Hydrolysis in pharmaceutical formulations. Pharm Dev Technol. 2002;7(2):113–46. https://doi.org/10.1081/PDT-120003494.

13. Carstensen JT. Effect of moisture on the stability of solid dosage forms. Drug Dev Ind Pharm. 1988;14(14):1927–69. https://doi.org/10.3109/03639048809151998.

14. Shah UV, Karde V, Ghoroi C, Heng JYY. Influence of particle properties on powder bulk behaviour and processability. Int J Pharm. 2017;518(1–2):138–54. https://doi.org/10.1016/j.ijpharm.2016.12.045.

15. Chen H, Aburub A, Sun CC. Direct compression tablet containing 99% active ingredient-a tale of spherical crystallization. J Pharm Sci. 2019;108(4):1396–400. https://doi.org/10.1016/j.xphs.2018.11.015.

16. Goh HP, Heng PWS, Liew CV. Comparative evaluation of powder flow parameters with reference to particle size and shape. Int J Pharm. 2018;547(1–2):133–41. https://doi.org/10.1016/j.ijpharm.2018.05.059.

17. Dendukuri D, Doyle PS. The synthesis and assembly of polymeric microparticles using microfluidics. Adv Mater. 2009;21(41):4071–86. https://doi.org/10.1002/adma.200803386.

18. Nelson AZ, Kundukad B, Wong WK, Khan SA, Doyle PS. Embedded droplet printing in yield-stress fluids. Proc Natl Acad Sci. 2020;117(11):5671. https://doi.org/10.1073/pnas.1919363117.

19. Yeap EWQ, Ng DZL, Prhashanna A, Somasundar A, Acevedo AJ, Xu Q, et al. Bottom-up structural design of crystalline drug-excipient composite microparticles via microfluidic droplet-based processing. Cryst Growth Des. 2017;17(6):3030–9. https://doi.org/10.1021/acs.cgd.6b01701.

20. Yeap EWQ, Ng DZL, Lai D, Ertl DJ, Sharpe S, Khan SA. Continuous flow droplet-based crystallization platform for producing spherical drug microparticles. Org Process Res Dev. 2018;23(1):93–101. https://doi.org/10.1021/acs.oprd.8b00314.

21. Leon RAL, Badruddoza AZM, Zheng L, Yeap EWQ, Toldy AI, Wong KY, et al. Highly selective, kinetically driven polymorphic selection in microfluidic emulsion-based crystallization and formulation. Cryst Growth Des. 2014;15(1):212–8. https://doi.org/10.1021/cg501222n.

22. Yeap EWQ, Acevedo AJ, Khan SA. Microfluidic extractive crystallization for spherical drug/drug-excipient microparticle production. Org Process Res Dev. 2019;23(3):375–81. https://doi.org/10.1021/acs.oprd.8b00432.

23. Erdemir D, Daftary V, Lindrud M, Buckley D, Lane G, Malsbury A, et al. Design and scale-up of a co-processing technology to improve powder properties of drug substances. Org Process Res Dev. 2019;23(12):2685–98. https://doi.org/10.1021/acs.oprd.9b00354.

24. Rosenbaum T, Erdemir D, Chang SY, Kientzler D, Wang S, Chan SH, et al. A novel co-processing method to manufacture an API for extended release formulation via formation of agglomerates of active ingredient and hydroxypropyl methylcellulose during crystallization. Drug Dev Ind Pharm. 2018;44(10):1606–12. https://doi.org/10.1080/03639045.2018.1483386.

25. Erdemir D, Rosenbaum T, Chang S-Y, Wong B, Kientzler D, Wang S, et al. Novel co-processing methodology to enable direct compression of a poorly compressible, highly water-soluble active pharmaceutical ingredient for controlled release. Org Process Res Dev. 2018;22(10):1383–92. https://doi.org/10.1021/acs.oprd.8b00204.

26. Schenck L, Erdemir D, Saunders Gorka L, Merritt JM, Marziano I, Ho R, et al. Recent advances in co-processed APIs and proposals for enabling commercialization of these transformative technologies. Mol Pharm. 2020;17(7):2232–44. https://doi.org/10.1021/acs.molpharmaceut.0c00198.

27. Nelson AZ, Xie J, Khan SA, Doyle PS. Continuous embedded droplet printing in yield-stress fluids for pharmaceutical drug particle synthesis. Advanced Materials Technologies. 2021;6(4):2001245. https://doi.org/10.1002/admt.202001245.

28. Fortt R, Tona R, Martin-Soladana PM, Ward G, Lai D, Durrant J, et al. Extractive crystallization of cabotegravir in droplet-based microfluidic devices. J Cryst Growth. 2020;552:125908. https://doi.org/10.1016/j.jcrysgro.2020.125908.

29. Nisisako T, Ando T, Hatsuzawa T. High-volume production of single and compound emulsions in a microfluidic parallelization arrangement coupled with coaxial annular world-to-chip interfaces. Lab Chip. 2012;12(18):3426–35. https://doi.org/10.1039/c2lc40245a.

30. Xu J, Singh V, Yin X, Singh P, Wu L, Xu X, et al. Solvents effects on crystallinity and dissolution of beta-artemether(). Drug Dev Ind Pharm. 2017;43(3):372–8. https://doi.org/10.1080/03639045.2016.1253728.

31. Udoh CE, Garbin V, Cabral JT. Microporous polymer particles via phase inversion in microfluidics: impact of nonsolvent quality. Langmuir. 2016;32(32):8131–40. https://doi.org/10.1021/acs.langmuir.6b01799.

32. Tu Y. Artemisinin—a gift from traditional Chinese medicine to the world (Nobel Lecture). Angew Chem Int Ed. 2016;55(35):10210–26. https://doi.org/10.1002/anie.201601967.

33. World Health Organization: Model List of Essential Medicines. https://list.essentialmeds.org/ (2020). Accessed 29 June 2020.

34. Arribas Bueno R, Crowley CM, Davern P, Hodnett BK, Hudson S. Heterogeneous crystallization of fenofibrate onto pharmaceutical excipients. Cryst Growth Des. 2018;18(4):2151–64. https://doi.org/10.1021/acs.cgd.7b01598.

35. International Council For Harmonisation Of Technical Requirements For Pharmaceuticals for Human Use. IMPURITIES: GUIDELINE FOR RESIDUAL SOLVENTS Q3C(R8). https://database.ich.org/sites/default/files/ICH_Q3C-R8_Guideline_Step4_2021_0422_1.pdf (2021). Accessed 3 Dec 2021.

36. Zhang Y, Liu QZ, Zhang DK, Jiang YB. Polymorphism, crystal structure and crystal habit of β-artemether. Huagong Xuebao/CIESC J. 2011;62:2958–63. https://doi.org/10.3969/j.issn.0438-1157.2011.10.040.

37. Nair NR, Sekhar VC, Nampoothiri KM, Pandey A. 32 - Biodegradation of biopolymers. In: Pandey A, Negi S, Soccol CR, editors. Current developments in biotechnology and bioengineering. Elsevier; 2017. p. 739–55.

38. Clancy D. 13 - Continuous secondary process selection and the modeling of batch and continuous wet granulation. In: Pandey P, Bharadwaj R, editors. Predictive modeling of pharmaceutical unit operations. Woodhead Publishing; 2017. p. 343–81.

39. Schulze D. Flow properties of bulk solids. In: Schulze D, editor. Powders and bulk solids: behavior, characterization, storage and flow. Berlin, Heidelberg: Springer Berlin Heidelberg; 2008. p. 35–74.

40. Ketterhagen WR, Curtis JS, Wassgren CR, Hancock BC. Predicting the flow mode from hoppers using the discrete element method. Powder Technol. 2009;195(1):1–10. https://doi.org/10.1016/j.powtec.2009.05.002.

41. Hansen DL, Tulinius D, Hansen EH. Adolescents' struggles with swallowing tablets: barriers, strategies and learning. Pharm World Sci. 2007;30(1):65. https://doi.org/10.1007/s11096-007-9142-y.

42. Marconati M, Raut S, Burbidge A, Engmann J, Ramaioli M. An in vitro experiment to simulate how easy tablets are to swallow. Int J Pharm. 2018;535(1):27–37. https://doi.org/10.1016/j.ijpharm.2017.10.028.

43. Friedman M, Donbrow M. Fluidized bed coating technique for production of sustained release granules. Drug Dev Ind Pharm. 1978;4(4):319–31. https://doi.org/10.3109/03639047809060846.

44. Yadavali S, Jeong H-H, Lee D, Issadore D. Silicon and glass very large scale microfluidic droplet integration for terascale generation of polymer microparticles. Nat Commun. 2018;9(1):1222. https://doi.org/10.1038/s41467-018-03515-2.